LAWRENCE
LIVERMORE
NATIONAL
LABORATORY

UCRL-PROC-227311

Aluminum Rayleigh Taylor Strength Measurements and Calculations

M. J. Lindquist, R. M. Cavallo, K. T. Lorenz, S. M. Pollaine, B. A. Remington, V. A. Raevsky

January 18, 2007

10th International Workshop on the Physics of Compressible Turbulent Mixing
paris, France
July 16, 2006 through July 21, 2006

-e-mail: lindquist8@llnl.gov

Aluminum Rayleigh Taylor Strength Measurements and Calculations

M.J. Graham LINDQUIST[1], R.M. CAVALLO[1], K.T. LORENZ[1], S.M. POLLAINE[1], B.A. REMINGTON[1] and V.A. RAEVSKY[2]

[1]LAWRENCE LIVERMORE NATIONAL LABORATORY 7000 East Avenue Livermore California 94550
[2]RUSSIAN FEDERAL NUCLEAR CENTER - VNIIEF, Sarov, Russia

Abstract: A traditional approach to the study of material strength has been revitalized at the Russian Federal Nuclear Center (VNIIEF). Rayleigh Taylor strength experiments have long been utilized to measure the material response of metals at high pressure and strain rates. A modulated (sinusoidal or sawtooth perturbation) surface is shocklessly (quasi-isentropically) accelerated by a high explosive (HE) driver, and radiography is used to measure the perturbation amplitude as a function of time. The Aluminum T-6061 targets are designed with several sets of two-dimensional sawtooth perturbations machined on the loading surface. The HE driver was designed to reach peak pressures in the range of 200 to 300 kbar and strain rates in the range of 10^4 - 10^6 s^{-1}. The standard constitutive strength models, Steinberg-Guinan (SG) [1], Steinberg-Lund (SL) [2], Preston-Tonks-Wallace (PTW) [3], Johnson-Cooke (JC) [4], and Mechanical Threshold Stress (MTS) [5], have been calibrated by traditional techniques: (Hopkinson-Bar, Taylor impact, flyer plate/shock-driven experiments). The VNIIEF experimental series accesses a strain rate regime not attainable using traditional methods. We have performed a detailed numerical study with a two-dimensional Arbitrary Lagrangian Eulerian hydrodynamics computer code containing several constitutive strength models to predict the perturbation growth. Results show that the capabilities of the computational methodology predict the amplitude growth to within 5 percent of the measured data, thus validating both the code and the strength models under the given conditions and setting the stage for credible future design work using different materials.

1 INTRODUCTION

The evolution of a Rayleigh Taylor Instability (RTI) in metals has long been used to study and understand material strength under high pressure and high loading rates [6-9]. Under aggressive loading conditions, material strength serves to stabilize or retard instability-induced perturbation growth. An RTI occurs at a perturbed surface of a metal that has been accelerated by another material of a lower density. In Figure 1, a material (ρ_H) having a uniform frequency of small amplitude perturbations, with fixed wavelength, λ, is accelerated by low density, high--explosive (HE) products (ρ_L). Rather than uniform compression of the material surface, stress gradients are formed which induce plastic flow. Material moves from the valleys into the spike regions, increasing the amplitude of the original modulation. Spike growth continues, with increasing time, as illustrated in Figure 1. To assess the effect of material strength under RTI conditions, the evolution of the perturbation growth is used as a metric.

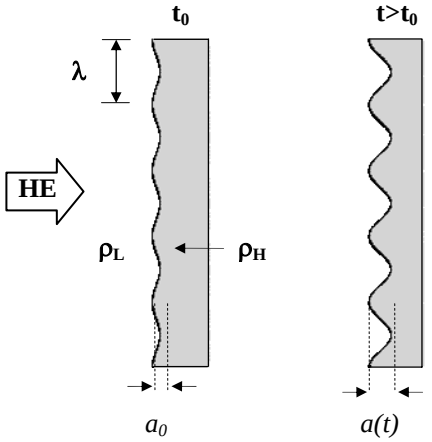

Figure 1. Schematic of RTI. a_0 is the initial amplitude of the perturbation, peak to valley. *A(t)* shows perturbation growth at later time.

During the decades that material strength has been studied, numerous experimental techniques have been developed to measure strength properties as functions of strain, pressure, temperature and strain rate. The data from Hopkinson-bar, Taylor impact and flyer plate/shock-driven experiments have all been used to formulate and validate constitutive strength models (SG, PTW, JC, MTS) widely in use in current hydrocodes. These experiments have largely been applied to physical problems where the strain and strain rate regimes are mostly less than 100 percent and less than 10^4 s^{-1}, respectively. There are many applications where the RTI-induced strain exceeds 100 percent and strain rates are in the 10^4 – 10^8 s^{-1} range, for example, RTI in Inertial Confinement Fusion applications.

The VNIIEF RTI growth experiments are serving to provide the data necessary to validate existing strength models in the strain and strain rate regimes mentioned. The RTI growth experiments revitalized at VNIIEF are a technique initiated by Barnes, et al [6]. Barnes' idea is to smoothly accelerate a sinusoidally perturbed surface by the expansion of HE products across a void thus guaranteeing shockless (quasi-isentropic) loading to pressures in the hundreds of kilobar range. What we have investigated are a series of experiments which have attained 200 – 300 kbar peak pressures and strain rates in the range of 10^4 s^{-1} - 10^6 s^{-1}. This is the first time since Barnes' [6] pioneering work in 1974 that experiments of this kind have been accomplished. We have performed a detailed numerical study to predict the perturbation amplitude using two constitutive strength models, namely, SG and PTW. The remainder of the article is dedicated to details of the experimental technique, the numerical results and justification for follow-on experiments at higher pressures and strain rates using different materials.

2 EXPERIMENTAL CONFIGURATION

The experimental setup is based on the original series of experiments formulated by Barnes [6] for the purpose of studying the growth (or lack thereof) of a sinusoidal perturbation imposed on a metal liner accelerated by HE products. It was shown that the perturbation growth is greatly moderated by the dynamic yield strength. In order to avoid the complications and heating caused by shock formation, the experiment was designed with a void between the HE driver and the target. The HE products cross the void and pile up on the side of the metal liner containing the small amplitude perturbations, providing a smooth rise to peak pressures. A schematic of the VNIIEF experimental design is provided in Figure 2.(a), (b), (c).

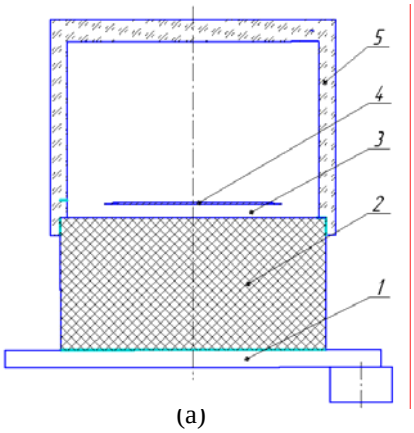

(a)

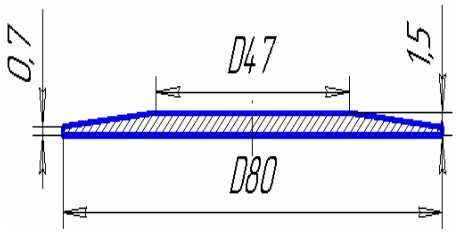

(b)

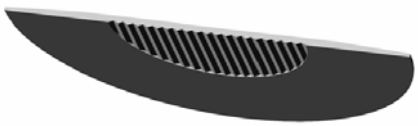

(c)

Figure 2. (a) Schematic of the experimental assembly (*1*) planar detonation wave generator, (*2*) HMX-based HE, (*3*) vacuum gap, (*4*) studied liner, Aluminum T-6061, and (*5*) sealing cylinder; (b) dimensions of aluminium liner; and (c) periodic perturbations machined on the loading surface of the aluminium.

The dimensions of the HE cylinder are diameter 120 mm and height 60 mm. The vacuum gap is fixed to be 3.5 mm. The aluminium sample was machined to a mean thickness of 1.5 mm in the central region, and had an overall diameter of 80 mm. The back side of the target is bevelled (such that the sample is thinner at the edges than in the center) in order to prevent bending due to lagging peripheral zones behind the central part of interest. The perturbations are located on the side of the target facing the HE. The composition of the HE governs the magnitude of the pressure. For the 300 kbar case, an HMX-based composition was used having density $\rho_0 = 1.885$ g/cm^3 and energy release Q = 6.1kJ/g. Results will also be shown for 200 kbar peak pressure, where a TNT/RDX-based composition was used having density $\rho_0 = 1.67$ g/cm^3 and energy release Q = 5.786 kJ/g. Due to the limitations of machining capabilities, the perturbations were chosen to be saw-tooth (Ideally, a sinusoidal modulation is preferred as it is considered a single frequency mode). For each of the liners studied, the wavelength of the perturbation, λ, is set at 2 mm. On each of the loading surfaces of the aluminium liners, a set of twenty wavelengths were machined. The perturbations are in two zones of 10 wave-

lengths each. The wavelength is fixed at λ = 2mm and the initial amplitude (peak to valley), A_0, in each of the zones of 10 are 0.06, 0.11, 0.15, 0.19, or 0.23 mm. Hence each sample provided information for two different initial perturbation amplitudes.

There were a total of seven experiments performed in this series, four of which were at 300 kbar peak pressure and three, at 200 kbar peak pressure. Perturbation growth was obtained by x-radiography; therefore, only one piece of data can be obtained from one experiment. A broad-band x-ray source having peak energies of 1 MeV and pulse widths of 100 ns (fwhm) was used in a side-on imaging arrangement. A sample of the X-ray photos of the aluminium liner at 300 kbar peak pressure is provided in Figure 3.

Zone	λ, mm	A_0, mm	S, mm	X-ray photo of studied plate	A, mm
a) b)	2 2	0.11±0.01 0.15±0.01	11±0.5	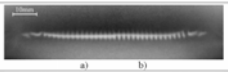	1±0.13 2.13±0.18
a) b)	2 2	0.06±0.01 0.11±0.01	11±0.5	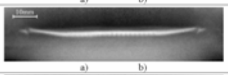	0.63±0.1 0.9±0.09
a) b)	2 2	0.11±0.01 0.15±0.01	6.9±0.5	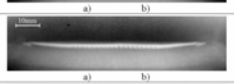	0.72±0.09 1.24±0.10
a) b)	2 2	0.06±0.01 0.15±0.01	12±0.5	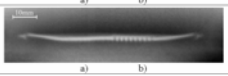	0.4±0.09 1.96±0.14

Figure 3. X-ray results from aluminum experiments with peak pressures to 300 kbar. Sections a) and b) represent the zones of different initial perturbation amplitude. S (mm) is the position of the liner for a given x-ray image. A_0 (mm) is the initial peak to valley perturbation amplitude. A (mm) is the amplitude of the perturbation at the given position.

3 COMPUTATIONAL TECHNIQUE

A. Characterization of the Drive

Material strength is inferred from the RTI; however, it is critically important to correctly model the drive, or acceleration source of the aluminium liner, in order to accurately extract the material strength. The driver of the acceleration for the RTI comes from the stored chemical energy released from the HE, and therefore, the characterization of the pressure source is an integral part of the process. The JWL [10] equation of state, Equation (1), is a pressure-volume-energy equation most commonly and successfully used in the hydrocodes, where P is the pressure, ν is the relative volume, related by $\nu = V/V_0$, and V_0 is the initial volume, V, the time-evolved volume; A, B, R_1, R_2 and ω are constants. The parameters used for each HE are given in Figure 4.

$$P = A\left(1-\frac{\omega}{R_1\nu}\right)e^{-R_1\nu} + B\left(1-\frac{\omega}{R_2\nu}\right)e^{-R_2\nu} \quad (1)$$

	HMX	TNT/RDX
ρ_0 (g/cc)	1.885	1.67
A (Mbar)	8.478669	5.008074
B (Mbar)	0.2195808	0.1687606
R	4.50	4.50
R_2	1.50	1.50
ω	0.35	0.32
E_0 (Mbar)	0.1088	0.0873
Γ_0+1	3.814231	3.885124
U_s (cm/μs)	0.9000	0.7600

Figure 4. JWL parameters for HE

We performed a detailed one-dimensional (1D) numerical study to characterize the drive conditions, comparing the Pressure, Velocity and Position versus time with the gas dynamic calculations provided by VNIIEF for both HE drive conditions. An analytic equation of state was used for the Aluminum T-6061, with two different strength models: SG and PTW. Figure 5 shows that the 1D ARES SG calculations are in good agreement with the VNIIEF 1D representation. Calibration tests for the drive were performed by VNIIEF using thicker aluminium and incorporating manganin gauges to obtain in-situ pressure data. Velocimetry was not available at the time. Figure 5. (a) (b) (c) shows good agreement between the ARES calibration model and the VNIIEF drive characterization for the pressure, velocity and position of the loading surface of the aluminium versus time.

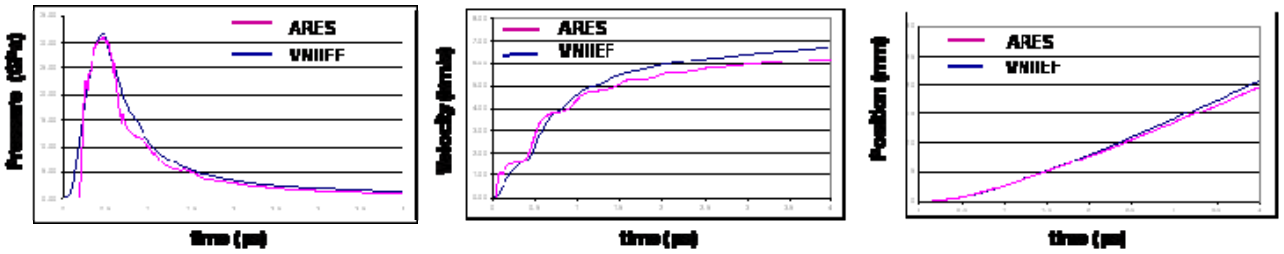

(a) (b) (c)

Figure 5. Comparision between ARES and VNIIEF drive conditions at the loading surface of the aluminium for the 300 kbar peak pressure experiments. (a) Pressure (GPa) vs. time (μs), (b) Velocity (km/s) vs. time (μs), and (c) Position vs. time (μs).

Very good agreement is shown at early time during the calculation, approximately 1 μs into the problem, with the deviation at late time being due to the material strength. The material strength consumes energy and helps to decelerate the plate.

B. Calculated two-dimensional Perturbation Growth

The initial conditions for the two-dimensional (2D) simulations were modelled after the experiment (Figure 6), using the drive calibrated in the 1D study. The full 2D calculations were performed using ARES, which is a massively parallel, multi-physics code. It is built on a multi-block Arbitrary Lagrangian Eulerian (ALE) hydrodynamics package and contains a wide array of physics models necessary for carrying out the HE driven material characterization experiments.

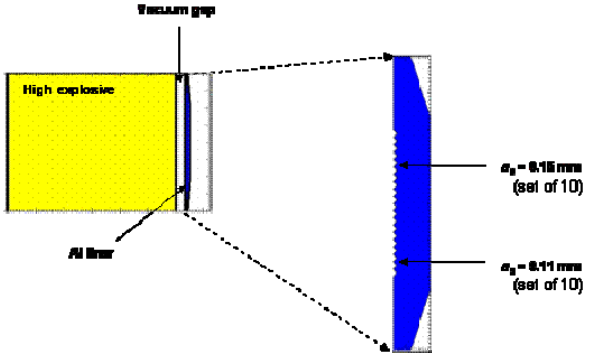

Figure 6. Schematic of the full 2D computational model, HE slab, vacuum gap and aluminium liner.

Each of the experiments was modelled with 120 zones per wavelength, with square zoning in the target, i.e., $\Delta x=\Delta y=1.67$ microns zoning in the metal. An analytic equation of state is used for the Aluminum T-6061. Two constitutive strength models were used to determine the material strength: Steinberg-Guinan [1] and Preston-Tonks-Wallce [3]. The SG model is an empirically based constitutive model with no explicit strain-rate dependence. Because of this feature, there has been some debate pertaining to the strain-rate regime in which SG is applicable. The SG equations are given in (2), (3), (4).

$$Y = Y_o f(\varepsilon_p) G(P,T)/G_o \qquad (2)$$

$$Y_o f(\varepsilon_p) = Y_o\left[1+\beta(\varepsilon_p+\varepsilon_i)\right]^n \le Y_{\max} \qquad (3)$$

$$G(P,T) = G_o\left[1+AP/\eta^{\frac{1}{3}} - B(T-300)\right] \qquad (4)$$

With *A* and *B* given,

$$A = \frac{1}{G_0}\frac{dG}{dP}$$

$$B = \frac{1}{G_0}\frac{dG}{dT}$$

$$\hat{\tau} = \hat{\tau}_s + \frac{S_0-\hat{\tau}_y}{p}\ln\left[1-\left[1-\exp\left(-p\frac{\hat{\tau}_s-\hat{\tau}_y}{S_0-\hat{\tau}_y}\right)\right]\exp\left\{-\frac{p\theta_0\psi}{(S_0-\hat{\tau}_y)\left[\exp\left(p\frac{\hat{\tau}_s-\hat{\tau}_y}{S_0-\hat{\tau}_y}\right)-1\right]}\right\}\right] \qquad (5)$$

$$\hat{\tau}_s = \max\left\{S_0-(S_0-S_\infty)\operatorname{erf}\left[\kappa\hat{T}\ln\left(\frac{\gamma\dot{\xi}}{\dot{\psi}}\right)\right], S_0\left(\frac{\dot{\psi}}{\gamma\dot{\xi}}\right)^{\beta}\right\} \qquad (6)$$

$$\hat{\tau}_y = \max\left\{y_0-(y_0-y_\infty)\operatorname{erf}\left[\kappa\hat{T}\ln\left(\frac{\gamma\dot{\xi}}{\dot{\psi}}\right)\right], \min\left[y_1\left(\frac{\dot{\psi}}{\gamma\dot{\xi}}\right)^{y_2}, S_0\left(\frac{\dot{\psi}}{\gamma\dot{\xi}}\right)^{\beta}\right]\right\} \qquad (7)$$

From shock wave experiments, it is often assumed that SL applies to strain rates up to 10^5 s^{-1}, beyond which SG applies and the strain rate becomes unimportant. Our calculations for Aluminum T-6061 using the SG constitutive model are shown in Figure 7. The PTW model (Equations 5, 6 and 7) is a physically based constitutive model with a thermal activation to phonon drag transition that takes effect at a specified strain rate in the 10^6 - 10^8 s^{-1} regime. Due to the scale-invariant nature of the PTW model, the authors claim it is valid for arbitrary strains, temperatures and strain rates [15]. The calculations for Aluminum T-6061 using the PTW strength model are also shown in Fig. 7. Simulations with either model (SG vs PTW) reproduce the observed results reasonably well.

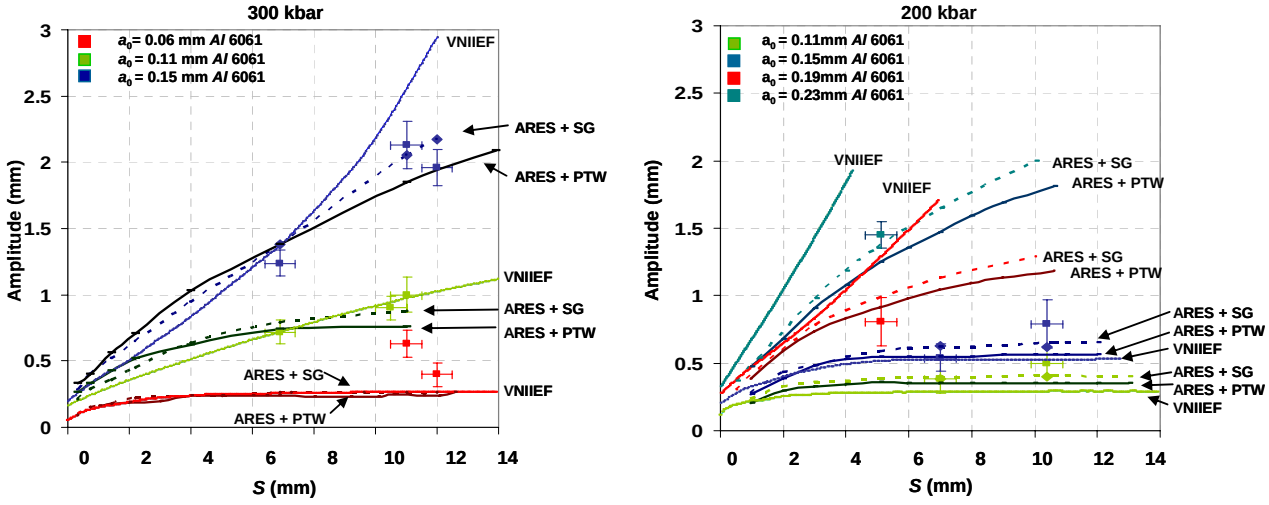

(a) (b)

Figure 7. Perturbation amplitude vs. distance travelled. (a) P_{max} = 300 kbar (HMX driver), and (b) P_{max} = 200 kbar (TNT/RDX driver).

The results shown in Figure 7 represent the data from the seven experiments, VNIIEF calculations with their own model, ARES calculations with SG strength model and ARES calculations with PTW strength model. The ARES 2D simulations have predicted the material yield strength to within 5 percent of the measured data for all cases except the smallest initial amplitude case. The standard input parameters for the SG and PTW models were used for Aluminum T-6061. Since Aluminum T-6061 is a well-known substance, it is not surprising to find such good agreement. However, the fact that both of the material strength models were formulated from data with very different experimental techniques and strain less than 100 percent indicates that the strength models for Aluminum T-6061 implemented in our hydrocodes are well calibrated. These experiments have provided an excellent validation experimental set for Aluminum T-6061 in the given conditions.

We show in Fig. 8 predictions from the PTW model for flow stress for Al6061 at the representative conditions of P = 200 kbar, T = 400 K, ρ/ρ_0 = 1.1, ε = 0.1 (solid curve). [11] Flow stress is plotted versus log($d\varepsilon/dt$). The flow stress has been normalized by the value predicted by PTW at $d\varepsilon/dt$ = 1 (but still at the above P, T, ρ/ρ_0, and ε). Also plotted is the result for thermal activation only (dashed) curve, turning off the contribution due to nonlinear phonon drag. In the thermal activation regime, PTW predicts flow stress increasing logarithmically with strain rate, $\sigma \sim \ln(d\varepsilon/dt)$, whereas in the nonlinear phonon drag regime, PTW assumes a power law dependence on strain rate, $\sigma \sim (d\varepsilon/dt)^{\beta}$, with $\beta \sim 1/4$. Note, using nominal input parameters for Al6061 for the PTW model, the transition from thermal activation to phonon drag occurs at strain rates of ~10^8 s^{-1}. Hence, the PTW model predicts that these HE-RT experiments, with strain rates in the 10^4-10^6 s^{-1} range, lie in the thermal activation regime. Also plotted in Fig. 8 (dotted curve) is the prediction from the SG model. The SG model is independent of strain rate, but is meant only for high strain rate applications, $d\varepsilon/dt > 10^4$ - 10^5 s^{-1}. Note also, for the conditions of these experiments, 10^4-10^6 s^{-1}, the PTW model predicts 10-20% greater strength, due to the strain rate dependence in the thermal activation regime. This is consistent with the simulated growth factors being slightly lower for the HE-RT experiments when the PTW model is used, compared to the SG model.

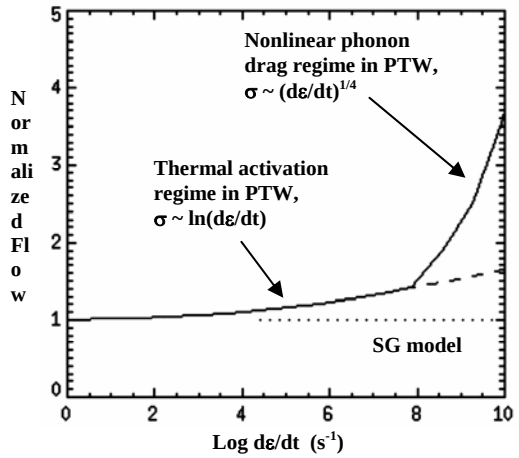

Figure 8. Normalized flow stress versus log(strain rate) from the PTW model versus the SG model.

There is a nearly 50 percent discrepancy between the calculations and the experimental data at 300 kbars for the smallest initial perturbation amplitude of 0.06 mm. We have found that this is due to the limitations of the machining accuracy. The VNIIEF machining error, at that time, was as much as 20 percent. We performed calculations incrementally increasing the initial amplitude from 0.06 mm to 0.08 mm and found good agreement when the initial perturbation amplitude has been arbitrarily set to 0.075 mm.

4 CONCLUSION

Modeling results show that the standard SG and PTW parameters for Aluminum T-6061 are sufficient to model the evolution of a RTI driven quasi-isentropically to pressures in the range 200 – 300 kbar, strain larger than 100 percent and strain rates to 10^6 s^{-1}. The simulated perturbation amplitude as a function of distance generally agrees well with the VNIIEF data. Future work will focus on higher pressures and strain rates, comparisons of BCC (such as vanadiuim) vs FCC (such as Al6061) materials, and different initial grain sizes. Understanding the effects of varying the peak pressure and strain rate is extremely important, to see how these constitutive models scale outside the regime in which they were calibrated.

ACKNOWLEDGEMENTS

The authors would like to thank Clark Souers of Lawrence Livermore National Laboratory for insight into the VNIIEF drive systematics, in particular, the characterization of the HE. We would also like to acknowledge the many interesting and insightful discussions with colleagues in our own laboratory and others: Patrick O. Egan, Elaine A. Chandler, Dana P. Rowley, Oleg Schilling, Henry D. Shay and M. Anthony Zocher. This work was performed under the auspices of the U.S. Department of Energy by the University of California Lawrence Livermore National Laboratory under Contract No. W-7405-Eng-48.

[1] D.J. Steinberg, S.G. Cochran and M.W. Guinan, J. Appl Phys. **51**, 1496 (1980).
[2] D.J. Steinberg and C.M. Lund, J. Appl Phys. **65**, 1528 (1989)
[3] D.L. Preston, D.L. Tonks, and D.C. Wallace, J. Appl Phys. **23**, 211 (2003).
[4] G.R. Johnson, J.M. Hoegfeldt, U.S. Lindholm and A. Nagy, ASME J Eng Mater Tech **105,** 42 (1983).
[5] P.S. Folansbee and U.F. Kocks, Acta metal, **36**, 81 (1988).
[6] J.F. Barnes, P.J. Blewett, R.G. McQueen, K.A. Meyer and D. Venable, J. Appl Phys. **45**, 727 (1974).
[7] J.D. Colvin, M. Legrand, B.A. Remington, G. Schurtz and S.V. Weber, J. Appl Phys. **93**, 5287 (2003).
[8] D.H. Kalantar, B.A. Remington, E.A. Chandler, J.D. Colvin, D. Gold, K. Mikaelian, S.V. Weber, L.G. Wiley, J.S. Wark, A.A. Hauer and M.A. Meyers, J. Impact Engineer., **23**, 409 (1999).
[9] K.T. Lorenz, M.J. Edwards, S.G. Glendinning, A.F. Jankowski, J. McNaney, S.M. Pollaine and B.A. Remington, Phys. Plasmas, **12**, 056309 (2005).
[10] private conversation C. Souers.
[11] private conversation J.D. Preston.